Echo-planar Imaging

Robert L. DeLaPaz, MD

Echo-planar imaging is a fast magnetic resonance (MR) imaging technique that allows acquisition of single images in as little as 20 msec and performance of multiple-image studies in as little as 20 seconds. Echo-planar imaging achieves its speed by obtaining all spatial-encoding information after a single radio-frequency (RF) excitation. Conventional imaging requires multiple-RF excitations, separated by the repetition time (TR), to acquire this information. An "infinite" TR, routine lipid suppression, and sensitivity to magnetic susceptibility are other features of echo-planar imaging. Standard pulse sequences are used to obtain echo-planar images, which have diagnostic utility similar to that of conventional MR images. Echo-planar imaging is less sensitive to motion than is conventional MR imaging and allows imaging of rapidly changing physiologic processes such as blood flow and kinetic activity. Echo-planar imaging is opening new areas of MR imaging research and clinical applications.

■ INTRODUCTION

Echo-planar imaging is a fast magnetic resonance (MR) imaging technique that allows acquisition of single images in as little as 20 msec and performance of multisection studies in 20–60 seconds. The major advantages of echo-planar imaging over conventional imaging are (*a*) reduced imaging time with the potential for improved patient throughput, (*b*) reduced motion artifact, and (*c*) the ability to image rapid physiologic and kinetic processes. These capabilities are opening new fields of study for MR imaging, such as evaluation of cerebral perfusion, diffusion, and functional activation; evaluation of cardiac perfusion; rapid T1 and T2 calculation and diffusion imaging for tissue characterization; "MR fluoroscopy" of brain, cardiac, and joint motion; and potentially real-time MR monitoring of interventional procedures (1–8). This review will present the basic principles and features of echo-planar imaging and provide an introduction to its clinical and research applications, especially cerebral imaging.

Abbreviations: CBV = cerebral blood volume, FSE = fast spin echo, GRE = gradient echo, IR = inversion recovery, RF = radio frequency, SE = spin echo, S/N = signal-to-noise ratio, TE = echo time, TR = repetition time

Index terms: Magnetic resonance (MR), diffusion study, 10.12144 • Magnetic resonance (MR), echo planar, 10.121416 Magnetic resonance (MR), perfusion study, 10.12144 • Magnetic resonance (MR), physics

RadioGraphics 1994; 14:1045–1058

[1] From the Department of Radiology, Rm A1103, Memorial Sloan-Kettering Cancer Center, 1275 York Ave, New York, NY 10021. Received February 3, 1994; revision requested March 30 and received May 17; accepted May 18. **Address reprint requests to** the author.

© RSNA, 1994

■ BASIC CONCEPTS

To fully understand echo-planar imaging, one must be familiar with the concepts of gradient spatial encoding, k space, and k-space mapping (9, pp 3–9; 10).

• Gradient Spatial Encoding

Application of gradients across the object being imaged is the physical method of encoding spatial information in MR imaging (Fig 1). Applying a low-amplitude gradient (a gradient with a shallow slope) creates minimal phase warp across the object, allowing discrimination only between widely spaced points and thus encoding for low spatial frequencies and large structures. Applying a high-amplitude gradient (a gradient with a steep slope) creates greater phase warp across the object, allowing discrimination between closely spaced points and thus encoding for high spatial frequencies and small structures. The duration of the applied gradient also affects spatial frequency encoding. Short-duration gradients, like low-amplitude gradients, create minimal phase warp and thus encode low spatial frequencies. Long-duration gradients, like high-amplitude gradients, create greater phase warp and thus encode high spatial frequencies. The combination of gradient amplitude and duration determines the final spatial frequency encoding.

• K Space

K space is a coordinate system used to organize the gradient-derived spatial frequency information prior to the inverse Fourier transform and final image reconstruction (9, pp 3–9; 10–12) (Fig 2). Low spatial frequencies (large objects and image contrast) are encoded in the center of k space, and high spatial frequencies (small objects and fine detail) are encoded at the periphery. K space is not a grid that can be directly overlaid on the image. Each point in k space represents a spatial frequency over the entire image. For example, all large objects anywhere in the image are encoded at points in the center of k space, and all small objects anywhere in the image are encoded at the periphery of k space. The range of spatial frequencies in k space can also be thought of as coding for different degrees of edge definition. Collecting data only in the center of k space produces a low-resolution, blurry image with unsharp

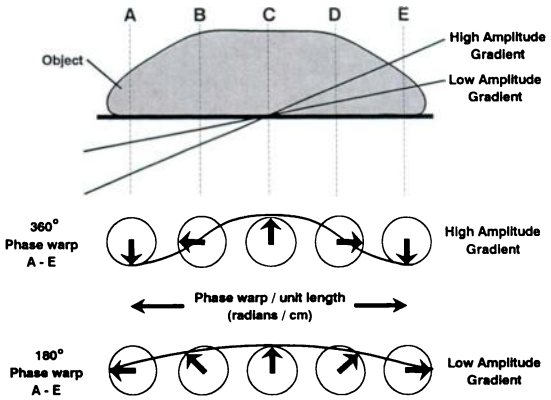

Figure 1. Diagram of gradient spatial frequency encoding. The spatial location of spins is given by their phase change along a gradient. Spatial frequency is defined as the spatial phase change or "phase warp" per unit length (in radians per centimeter) across the object being imaged. As gradient amplitude and duration increase, spatial frequency increases. (Adapted and reprinted, with permission, from reference 10.)

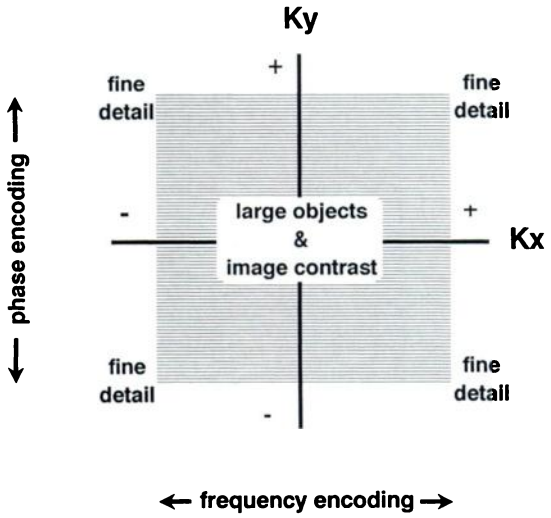

Figure 2. Diagram of k space.

edges, whereas adding data into the periphery produces a high-resolution image with sharp edge detail. Other important properties of this scheme are that points in the center of k space, which are collected at the peak intensity of the signal echo, dominate image contrast and the signal-to-noise ratio (S/N) but are sensitive to motion artifacts. Conversely, points at the periphery of k space, which are collected from less intense segments of the echo, have less effect on image contrast but determine maximum spatial resolution and noise in the image and produce less artifact from motion.

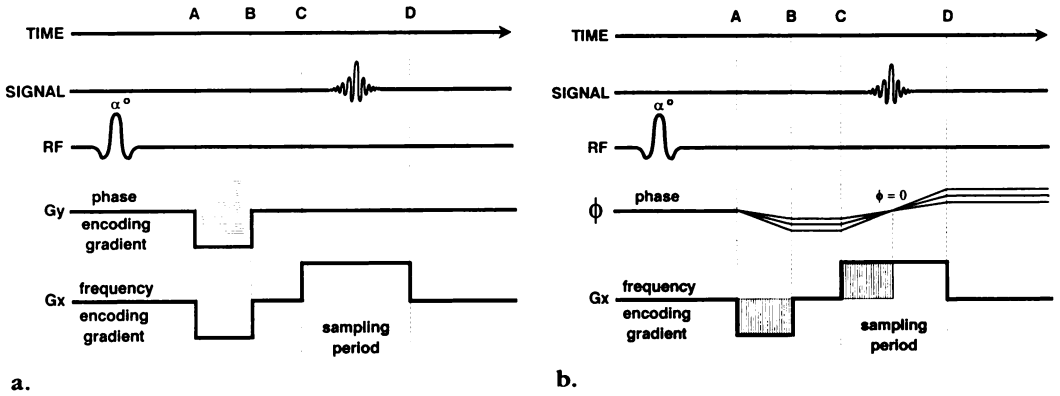

Figure 3. **(a)** Diagram of a conventional partial flip angle (α), gradient-echo (GRE) pulse sequence shows a typical pattern of in-plane gradient shifts used for spatial frequency encoding (with the section-select gradient ignored). During the first cycle of the pulse sequence, phase- and frequency-encoding gradients are initially switched simultaneously in the same direction (*A* to *B*). This is followed by no gradient application (*B* to *C*) and then an equal but opposite shift of the frequency-encoding or "read" gradient during the MR signal sampling period (*C* to *D*). The signal echo is generated by the sequence of opposing shifts of the frequency-encoding gradient. In subsequent pulse cycles, the frequency-encoding gradient shifts are the same, whereas the magnitude of the phase-encoding gradient is stepped through zero to an equal but opposite maximum. *RF* = radio frequency. **(b)** Diagram of gradient-induced phase change over time. The application of a gradient over time produces a divergence of spin phases (phase dispersion or dephasing) within the object being imaged (*A* to *B*). When the gradient is off, the separation of spin phases remains constant (*B* to *C*). A gradient shift in the opposite direction produces convergence of spin phases with rephasing at the center of the sampling period (Φ = 0), followed by dephasing (*C* to *D*). In GRE pulse sequences, this rephasing generates the MR signal echo. Spin-echo (SE) pulse sequences use a 180° RF pulse to rephase spins and generate the echo (Hahn echo). The echo signal is greatest at the point of rephasing and is progressively less on either side, where phase dispersion is present. The shaded areas under the gradients are equal and indicate that the degree of phase dispersion in the object is a function of gradient amplitude and duration (ie, the integral under the curve). (Adapted and reprinted, with permission, from reference 9.)

• K-space Mapping

The mapping of spatial frequency information in k space is derived from the history of gradient applications during image acquisition. As gradients are applied over time, the spatial frequency encoding changes and traces a trajectory through k space. These trajectories are precise records of the amplitude, duration, and direction of the applied gradients (Figs 3, 4). The simplest conventional method of k-space mapping is the application of gradients that encode all points across the frequency (x) direction with each pulse cycle whereas the phase (y) direction is encoded in single steps during successive cycles, separated by the TR interval. This accounts for the relatively long imaging times of conventional MR imaging. For example, acquisition of a single-excitation SE image with a 256 × 256 matrix (number of frequency points times number of phase steps) and a TR of 2,000 msec would require 8.5 minutes (one excitation × 256 phase steps × 2,000-msec TR). Faster imaging has been achieved on conventional imagers by using rapid acquisition with relaxation enhancement (RARE) or fast SE (FSE) techniques that map multiple (eg, 16) phase-encoding steps with each pulse cycle.

Figure 4. **(a)** Diagram of conventional k-space trajectory. The change in spatial frequency encoding produced by imaging gradients traces a trajectory through k space. The spatial frequency at any point during the pulse sequence can be thought of as the cumulative integral under the amplitude-duration curve along each gradient axis. The trajectory shown here is for the first cycle of the pulse sequence in Figure 3a. Prior to gradient applications, the encoded spatial frequency is zero, corresponding to the center of k space (*A*). The initial simultaneous phase and frequency gradient applications (dephasing lobes) shift spatial frequency equally in the *Kx* and *Ky* axes in the negative direction (*A* to *B*). With the gradients off, no additional phase is accumulated and thus no change in spatial frequency encoding occurs (*B* to *C*). Subsequent application of the frequency-encoding gradient alone, in the opposite direction, shifts spatial frequency through zero to a positive position along the *Kx* axis (*C* to *D*). This traversal parallels the signal echo envelope, with maximum signal at the center, where rephasing occurs, and lower signal at the periphery, where phase dispersion is greater. **(b)** Diagram of conventional k-space mapping. Repetition of the pulse sequence in Figure 3a generates a stepwise mapping of k space. The points along the *Ky* axis are produced by stepping the phase-encoding gradient from negative to positive during subsequent pulse cycles. Each step is separated in time by the repetition time (*TR*) interval. Total imaging time is given by the product of the number of excitations (*NEX*) acquired at each step, the TR, and the number of phase steps. When k space is symmetrically filled with spatial frequency data points, the two-dimensional inverse Fourier transform of the data generates the MR image.

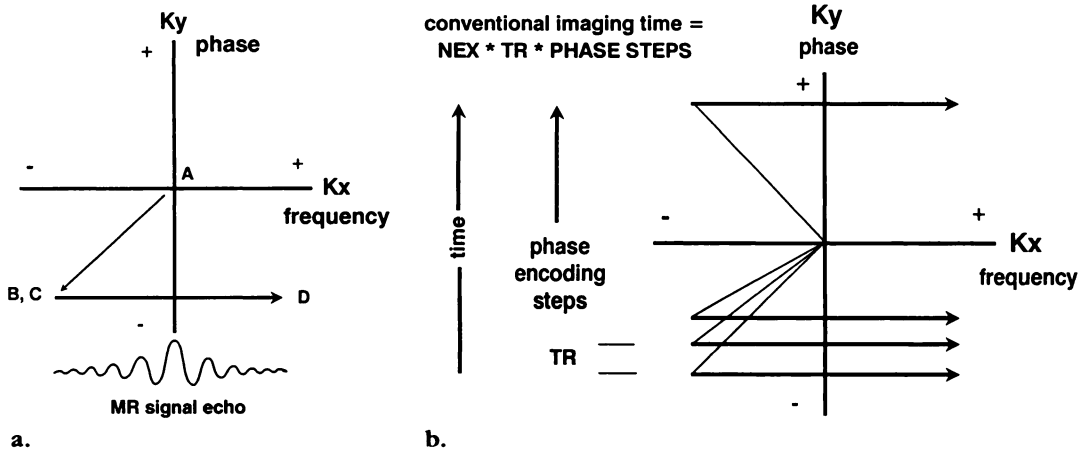

■ FEATURES

The key feature of echo-planar imaging that allows fast imaging is the use of rapid gradient switching to acquire all frequency-encoding points and all phase-encoding steps during a single pulse cycle (Fig 5). Echo-planar imaging was proposed in 1977 by Mansfield (15), who used a technique that combined an oscillating frequency-encoding gradient and a small, constant phase-encoding gradient applied during the free-induction decay following a single excitation pulse (16). Evolution of this technique improved k-space coverage and replaced the constant phase-encoding gradient with short-gradient-pulse "blips," resulting in the modulus-blipped echo-planar single-pulse technique (MBEST) (17). The first generation of whole-body echo-planar imaging hardware now in clinical use (Instascan; Advanced NMR Systems, Wilmington, Mass) is derived from the modulus-blipped echo-planar single-pulse method and acquires images by using rapid 1-kHz sinusoidal oscillation of the frequency-encoding gradient combined with blipping of the phase-encoding gradient at the zero-crossing points of the frequency-encoding gradient (5).

Figure 5. **(a)** Diagram of an echo-planar imaging SE pulse sequence shows echo-planar spatial encoding. A pre-encoding pulse is applied to both gradients between the RF pulses and prior to the MR signal sampling period (*A* to *B*). Rapid gradient switching is used to acquire all phase and frequency spatial-encoding points during one sampling period (*C* through *J*). This is done by oscillating the frequency-encoding gradient in a sinusoidal fashion and "blipping" the phase-encoding gradient at the zero-crossing points of the frequency-encoding gradient. Gradient echoes are generated within the SE envelope at the center of each lobe of the oscillating frequency-encoding gradient. Single-"shot" (single-acquisition) image data collection is reduced to the duration of the SE sampling period (as short as 20 msec). **(b)** Diagram of echo-planar k-space mapping shows the k-space trajectory traced by the echo-planar imaging (*EPI*) SE pulse sequence. Positive pre-encoding pulses are applied after the 90° RF excitation and displace the spatial frequency encoding an equal amount in each axis (*A* to *B*). The subsequent 180° inversion pulse flips the spatial-encoding point to the opposite corner of k space (*B* to *C*). Initial application of the frequency-encoding gradient alone causes horizontal displacement along the *Kx* axis (*C* to *D*). The positive pulse of the phase-encoding gradient at this point (*D*) steps up the trajectory, and the subsequent negative lobe of the oscillating frequency-encoding gradient generates a horizontal line in the opposite direction (*D* to *E*). This sequence is repeated throughout the sampling period (*C* through *J*) at the 1-kHz oscillation rate of the frequency-encoding gradient (500 μsec between each phase-encoding step). The result is a symmetric rectilinear trajectory through k space. Because there is no repetition of a single-shot image, the TR interval is infinite and is shown as open-ended in the figure. Multiple shots or multiple excitations (*NEX*) are separated by TR intervals. **(c)** Diagram of "mosaic" partial k-space mapping shows a "partial-read mosaic" scheme in which only part of k space is directly acquired (in two shots). Because k space is symmetrically redundant, these data can be "tiled" in a mosaic along the frequency-encoding or read axis and the rest of k space can be mathematically generated by means of conjugate synthesis. In this example, the resolution along the frequency-encoding axis is quadrupled, giving a final matrix of 512 × 128 (0.8 × 1.5-mm pixels). A "partial-phase mosaic" scheme obtains tile acquisitions vertically along the phase-encoding axis (with slight overlap at the center of k space) and allows shorter echo times (TEs) while maintaining high resolution. (Figure 5a–5c adapted and reprinted, with permission, from references 13 and 14.)

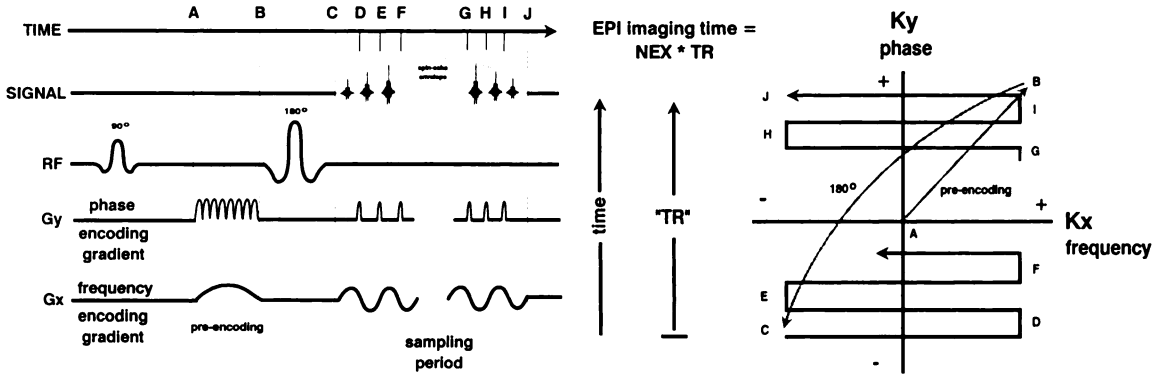

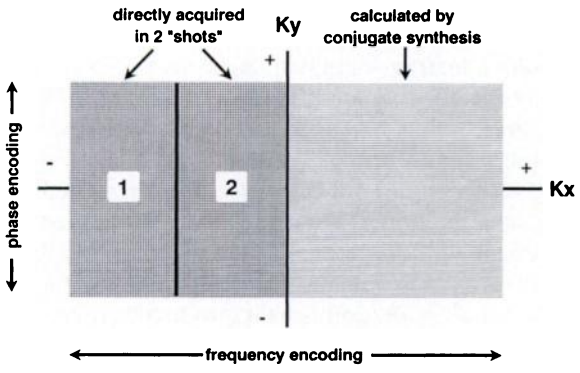

The simplest form of this method produces a symmetric rectilinear trajectory through k space with each acquisition or shot. Single-shot acquisition is the fastest type of echo-planar imaging acquisition (20–40 msec per image), but it limits spatial resolution (approximately 3 × 3-mm pixels with a matrix of 128 frequency points × 64 phase steps, a 40-cm [frequency] × 20-cm [phase] field of view, and 7-mm-thick sections). Higher-resolution single-shot images can be obtained with longer TEs (75 msec) and partial k-space mapping (eg, approximately 1.5 × 1.5-mm pixel resolution, 256 × 128 matrix, 5-mm-thick sections). The highest-resolution echo-planar images require two shots and a mosaic partial k-space mapping scheme (eg, approximately 0.8 × 1.5-mm pixels, 512 × 128 matrix, 5-mm-thick sections, 20 images obtained with four excitations in 49 seconds). Partial mapping schemes increase resolution by extending k space outward and include mapping of half or quarters of k space with extension to the remainder by using the mathematical technique of conjugate synthesis (13,18,19).

The S/N of echo-planar images is lower than that of conventional images with equal resolution because of the wide receiver bandwidth needed for fast data acquisition. S/N is proportional to the square root of the signal sampling time per pixel (with constant noise), and the sampling time per pixel is inversely proportional to the receiver sampling frequency bandwidth (9, pp 99 and 121). For example, encoding 128 points in 500 μsec (the time available for encoding all points across one line in k space with an idealized trapezoidal echo-planar imaging frequency-encoding gradient) allows only 3.9 μsec of sampling time for each point (each pixel). This translates to a nominal bandwidth of 256 kHz (128 samples divided by 0.0005 seconds) or 2,000 Hz per pixel. Conventional imagers typically sample 256 points in 8 msec, resulting in a sampling time per pixel of 31.25 μsec and a bandwidth of 32 kHz or 125 Hz per pixel. On the basis of the bandwidth differences alone, the S/N of echo-planar imaging is about one-third that of conventional imaging (ie, $[3.9/31.25]^{1/2} = 0.35$). For the Instascan system, the sinusoidal gradients produce nonlinear sampling, resulting in even shorter sampling times per pixel of 2.5 μsec ("unenhanced" mode) and 1.25 μsec ("enhanced" mode). In clinical use, the S/N of echo-planar imaging is actually closer to that of conventional imaging because of signal gains from the infinite TR and reduced noise from patient motion and imager instability (9, p 133). Loss of S/N at higher resolution in echo-planar imaging also may be compensated for by repeating the acquisition (increasing the number of excitations).

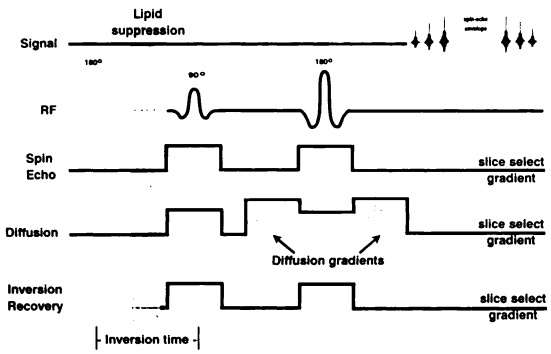

Figure 6. Diagram of three echo-planar imaging pulse sequences, with only the section-select gradients shown. The simplest is a standard SE sequence that generates signal and spatial information, as shown in Figure 5. The IR sequence adds a 180° inversion pulse prior to the SE component of the sequence. The diffusion sequence adds matching, stepped gradients on either side of the 180° inversion pulse. The second diffusion gradient recovers signal from static spins dephased by the first diffusion gradient. Signal is lost from spins that undergo motion-induced phase change between the gradients. (Adapted and reprinted, with permission, from references 13 and 14.)

Echo-planar images are obtained with standard MR pulse sequences, including SE, GRE, and inversion recovery (IR), and so allow fast imaging with retention of familiar tissue contrast characteristics (Fig 6). High-speed imaging on most conventional imagers is done with GRE, low-flip-angle techniques that have complex tissue contrast characteristics. Three unique features of echo-planar imaging also affect the appearance of images: the infinite TR, routine lipid suppression, and magnetic susceptibility sensitivity (5).

With single-shot echo-planar images, there is no repetition of the pulse cycle, so that the TR can be thought of as open-ended or infinite. This affects tissue contrast by eliminating the T1 partial saturation usually produced by repeating the pulse cycle in conventional sequences and so provides images that are truly T2 weighted. Multiple-shot or multiple-excitation echo-planar images, for which each successive shot or excitation is separated by a TR interval, show minimal saturation effects because TRs are usually much longer than in conventional imaging (eg, 4,000–8,000 msec). These infinite and long TR pulse sequences allow direct acquisition of T2-weighted GRE and SE images but not of T1-weighted SE images. T1-

weighted echo-planar images can be obtained with two other methods. The first involves reintroducing T1 partial saturation by adding a second, minimum TE SE excitation a short period after the initial SE pulse (eg, 500 msec). The price of this partial saturation method is a substantial reduction in S/N. The second involves use of an IR technique that adds a 180° pulse prior to the infinite TR sequence (Fig 6). The advantage of this method is that it preserves S/N, produces more strongly T1-weighted images than does the partial saturation method, and allows suppression of fat signal by use of an inversion time equal to the T1 of fat (13).

Routine lipid suppression, achieved by using a noninversion presaturation method, is routinely added to echo-planar imaging because the effective bandwidth per pixel in the phase-encoding direction is much smaller than the resonant frequency difference between fat and water (eg, 30 Hz per pixel vs a 225-Hz fat-water chemical shift at 1.5 T). If lipid signal were not suppressed, marked chemical shift artifact would be present, with displacement of fat signal from water signal by several centimeters (8 pixels or about one-eighth of a single-shot image). Water-suppressed images that show fat can be obtained separately.

The sensitivity of echo-planar imaging to magnetic susceptibility differences occurs for similar reasons. Like chemical shifts, magnetic susceptibility gradients between structures cause frequency shifts, which result in artifactual signal displacement and local image distortion. This effect is combined with signal loss caused by susceptibility gradient T2* shortening and appears most prominently at air-bone-tissue interfaces such as those at the paranasal sinuses, orbits, and petrous ridges in the head.

■ TECHNICAL REQUIREMENTS

The stringent technical requirements for echo-planar imaging have restricted its development until recently. Several researchers have recently demonstrated limited forms of echo-planar imaging on conventional MR imaging systems; these are multiexcitation interleaved methods that require multiple imaging cycles to acquire a complete image (20–22). However, the single-shot echo-planar imaging technique described here cannot be performed on current conventional MR imagers because of the need for higher magnetic field homogeneity, faster receivers, faster data processing, and faster and stronger gradients.

Maximum gradient amplitudes of 10 mT/m (1 G/cm) with rise times of about 600 μsec (amplitude/rise time = "slew rate" of 17 T/m per second) are typical of conventional imaging, but much higher slew rates are required for single-shot echo-planar imaging. The Instascan system uses gradients with a maximum amplitude of 25 mT/m and a rise time of 250 μsec (slew rate of 100 T/m per second) (1). Although this system uses resonant sinusoidal oscillation of the frequency-encoding gradient, echo-planar imaging systems now in development will likely use higher slew rates and trapezoidal waveforms with longer "flat tops" to improve spatial resolution (ie, extend k-space coverage along the frequency-encoding axis) (23). This will probably be achieved by means of new gradient-switching techniques and power supplies with use of nonresonant or hybrid resonant-nonresonant methods (eg, Catch and Hold; Advanced NMR Systems) (14). These techniques will allow tailored shaping of waveforms and extension of rapid gradient switching to other imaging methods, such as FSE and MR angiography (24,25).

Currently, single-shot clinical echo-planar imaging is implemented with hardware that is either single purpose and experimental or a specialized upgrade to a conventional MR imaging system, such as the Instascan system retrofit for the Signa (GE Medical Systems, Milwaukee, Wis) 1.5-T imager. On these retrofitted imagers, imaging can be done in either the echo-planar or the conventional mode. Clinical echo-planar imaging systems now in development will use multipurpose hardware capable of echo-planar imaging as well as faster conventional imaging, with gradient slew rates as high as 230 T/m per second (26).

■ SAFETY

Because rapidly changing magnetic field gradients may induce electrical currents in neural or cardiac tissue, concerns about the safety of echo-planar imaging have been raised. Two studies have demonstrated whole-body peripheral nerve stimulation at gradient-switching rates (dB/dt) of 63 and 86 T/sec, and the U.S. Food and Drug Administration has set its safety guideline at an upper limit of 60 T/sec for transverse gradients with a pulse width (the duration of a rectangular pulse or sinusoidal half period) of greater than 120 μsec (27–29). The Instascan system produces maximum transverse gradient-switching rates of 45 T/sec. Recent studies also indicate that cardiac stimulation thresholds are approximately 10 times higher than peripheral nerve stimulation thresholds and that sinusoidal gradient waveforms are more likely to produce peripheral nerve stimu-

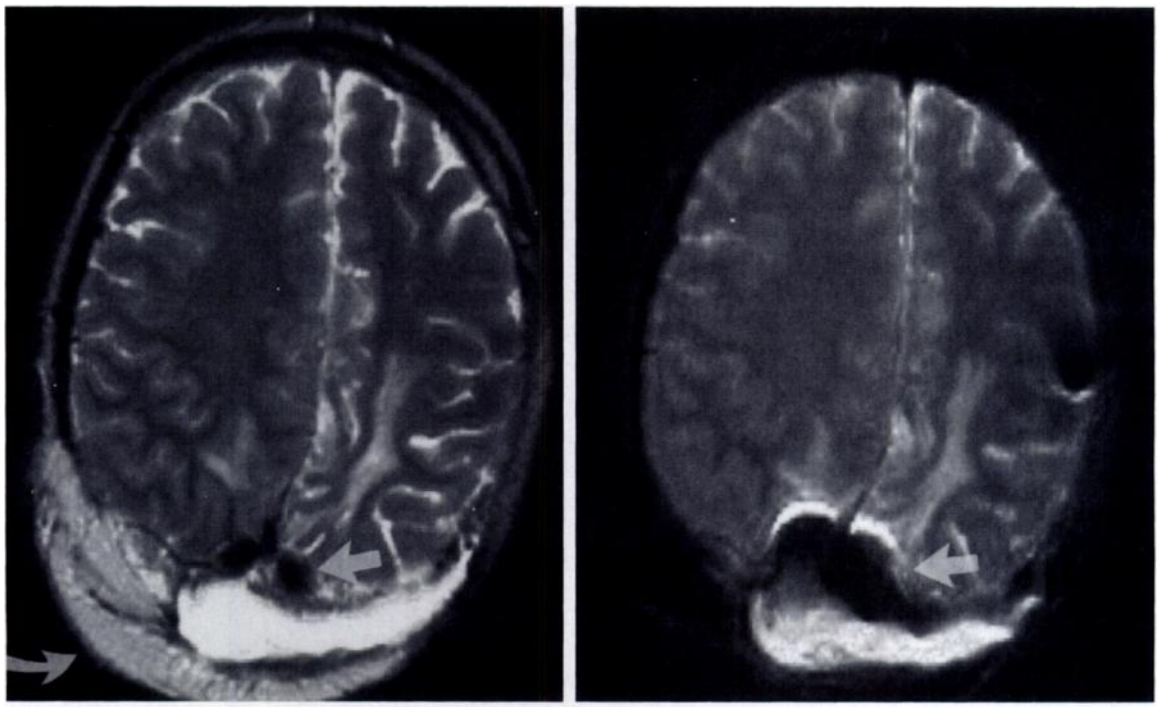

a. b.

Figure 7. Ferromagnetic artifact and lipid suppression. **(a)** Postoperative FSE T2-weighted axial image (3,650/102 [TR msec/TE msec], echo train of 8, 5-mm-thick sections, 2.5-mm gap, 256 × 192 matrix [0.9 × 1.1-mm pixels], one excitation) of the brain, acquired with a 1.5-T imager (Signa; GE Medical Systems) as part of a 20-image set obtained in 3 minutes 3 seconds, shows a scalp fat graft (curved arrow), a high-signal-intensity extraaxial fluid collection, and high-signal-intensity bilateral white matter edema. Two small areas of signal void represent ferromagnetic artifact from surgical clips (straight arrow). **(b)** Echo-planar SE T2-weighted axial image (4,000/75, 5-mm-thick sections, 2.5-mm gap, 512 × 128 matrix [0.8 × 1.5-mm pixels], four excitations, mosaic k-space mapping) of the brain, acquired with an echo-planar imaging system (Advanced NMR Systems) retrofit for a 1.5-T conventional imager (GE Medical Systems) as part of a 20-image set obtained in 49 seconds, matches the FSE image shown in **a** and shows the extraaxial fluid collection and white matter edema equally well. The scalp fat and fat graft are not seen because of the lipid suppression routinely used with echo-planar imaging. The ferromagnetic artifacts from the surgical clips are more prominent (arrow).

lation than are trapezoidal waveforms (30,31). Future echo-planar imaging systems, with trapezoidal gradients, will maintain high gradient-switching rates while staying well within biologic safety limits. RF power deposition in echo-planar imaging, as measured by means of the specific absorption rate (SAR), is generally equal to or less than in conventional imaging, while total energy deposition is much less due to the shorter imaging times (13). Acoustic noise is approximately 103 dB with the Instascan system at the 1-kHz oscillation rate of the frequency-encoding gradient but is effectively damped by standard earplugs.

■ APPLICATIONS

• Echo-planar versus Conventional MR Imaging

In general, clinical comparisons between echo-planar and conventional SE and FSE images of the brain have shown similar diagnostic utility (specificity, 0.96–1.00; sensitivity, 0.74–0.95 for T1-weighted and 0.81–0.92 for T2-weighted SE and FSE images) (32,33). Although the same lesions are seen in most cases, the S/N penalty and the T2* blurring with echo-planar imaging produce images that are subjectively judged as less sharp than SE or FSE images. However, the greater sensitivity of echo-planar images to magnetic susceptibility variations makes them more sensitive to small amounts of hemorrhage in tissue. Artifacts of different kinds affect echo-planar and conventional images about equally, with 7% of echo-planar T2-weighted images significantly degraded by ferromagnetic or magnetic susceptibility artifacts and 5% of FSE T2-weighted images significantly degraded by patient motion artifacts (32) (Figs 7–9). The advantage of echo-planar imaging in other areas is primarily its speed: Abdominal or chest images can be obtained without respiratory gating, with a shorter breath hold or no breath hold, and with no artifacts from peristalsis (Fig 10).

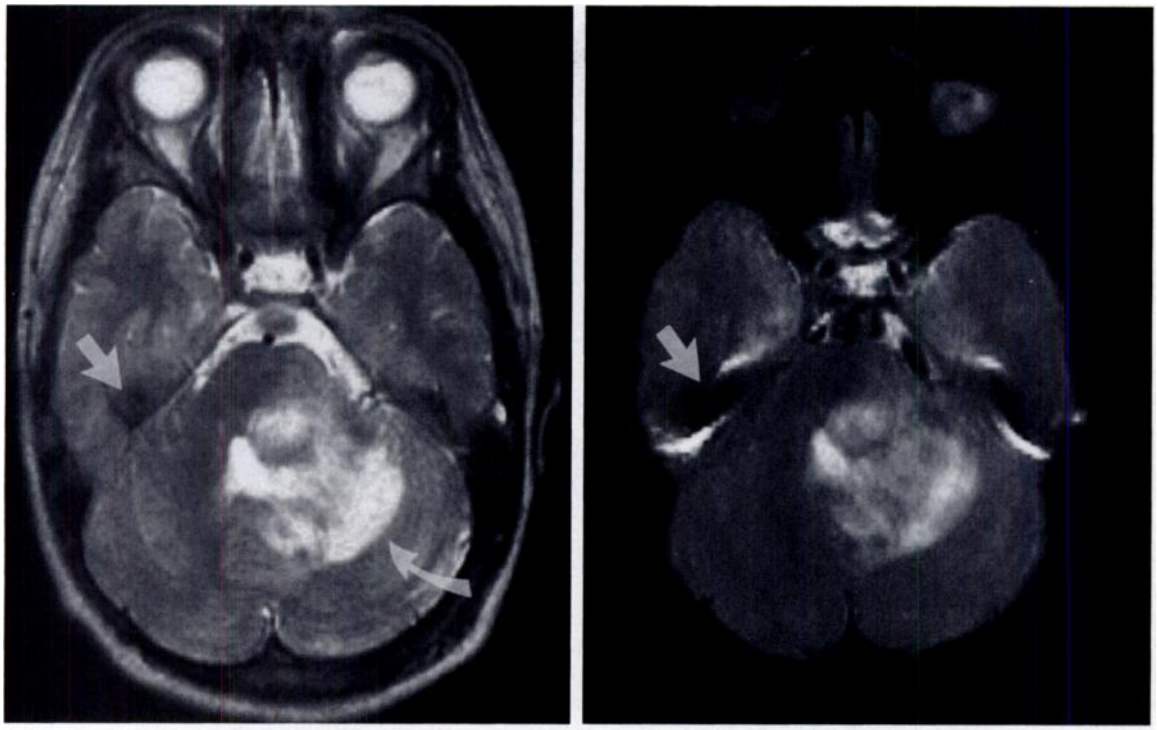

a. b.

Figure 8. Skull base magnetic susceptibility artifact. **(a)** FSE T2-weighted image, obtained as in Figure 7a, shows high signal intensity in a pontocerebellar neoplasm (curved arrow). Low signal intensity is seen at the apex of the petrous bone (straight arrow). **(b)** Echo-planar T2-weighted image, obtained as in Figure 7b, shows the high-signal-intensity pontocerebellar lesion well but also shows more prominent magnetic susceptibility artifact at the ridges of the petrous bone (arrow).

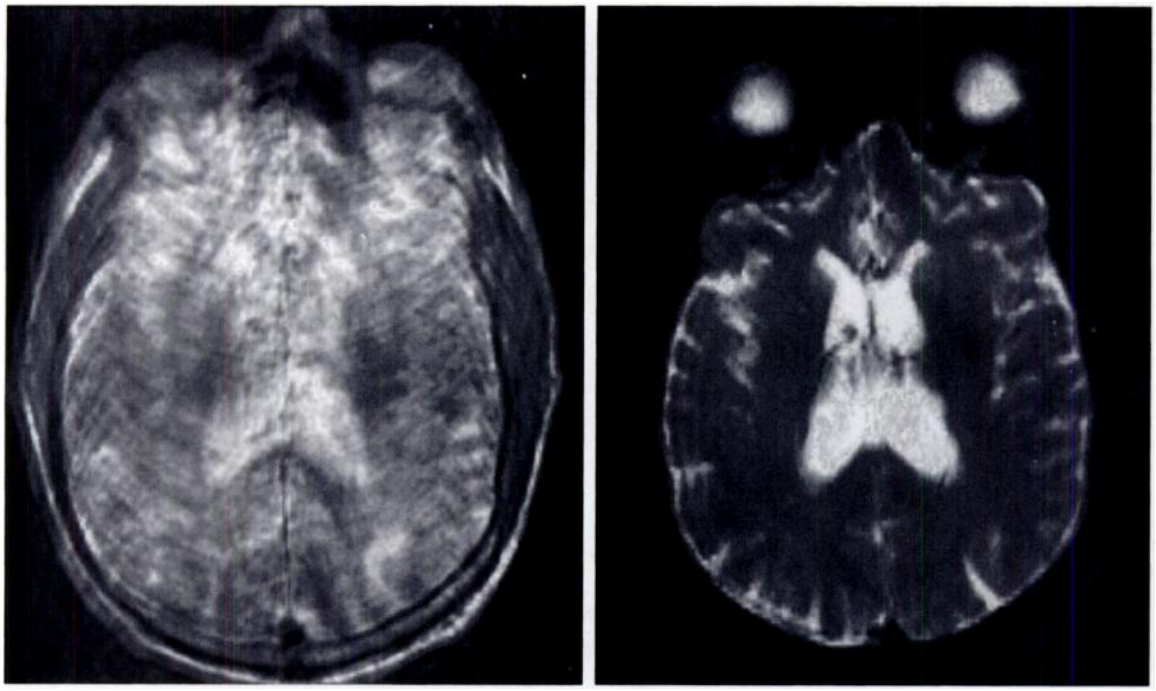

a. b.

Figure 9. Motion artifact in the head. **(a)** FSE T2-weighted image, obtained as in Figure 7a, shows marked degradation from patient motion, rendering the image nondiagnostic. **(b)** Echo-planar T2-weighted image, obtained as in Figure 7b within 5 minutes of the FSE image shown in **a**, is of diagnostic quality and shows no motion artifact.

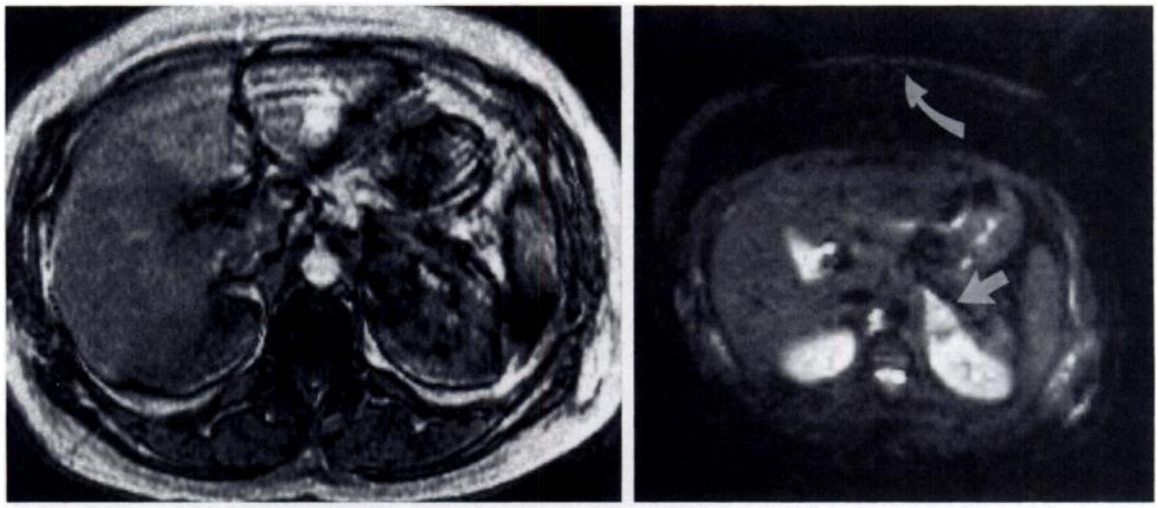

a. b.

Figure 10. Motion artifact in the abdomen. **(a)** GRE axial image (87/2.4, 8-mm-thick sections, 256 × 128 matrix [1 × 2-mm pixels], two excitations) of the abdomen, obtained with a 1.5-T imager (Signa; GE Medical Systems) as part of a multisection fast multiplanar spoiled gradient (FMPSPGR) acquisition performed in 23 seconds during a single breath hold, shows moderate motion degradation and no clear abnormality. **(b)** Echo-planar single-shot axial image (6,000/40, 10-mm-thick sections, 128 × 128 matrix [3 × 3-mm pixels], one excitation) of the abdomen, obtained with an echo-planar imager (Instascan ISSTEP; Advanced NMR Systems) as part of a stepped TE (four-TE) multishot acquisition performed in 23 seconds during a single breath hold, shows a left adrenal mass (straight arrow) not seen on the conventional GRE image **(a)**. Note the absence of signal from fat in the abdomen. The area of faint curvilinear signal intensity (curved arrow) anterior to the abdomen is the chemical shift artifact of incompletely suppressed lipid signal. T2s calculated from this stepped TE acquisition may help discriminate between benign and malignant adrenal masses (5).

Imaging of pediatric and uncooperative patients can be improved by reducing imaging time and decreasing or eliminating sedation.

• Functional Imaging

The most rapid development of echo-planar imaging applications is in the area of perfusion, diffusion, and functional MR imaging of the brain (34) (Figs 11, 12). Three techniques for monitoring regional cerebral blood perfusion have been demonstrated:

1. The first method measures relative CBV by means of the signal loss from T2* and T2 shortening resulting from perivascular magnetic susceptibility gradients created by an intravascularly administered bolus of paramagnetic contrast material (gadopentetate dimeglumine [formerly known as Gd-DTPA] or dysprosium-diethylenetriaminepentaacetic acid [Dy-DTPA]) (37). This method has been used primarily to map CBV changes in cerebral tumors and ischemia. In cerebral tumors, CBV appears to correlate positively with glioma tumor grade, probably because angiogenesis in actively growing tumors increases the tumor tissue blood volume (38). Areas of reduced CBV in cerebral ischemia closely match areas of reduced tissue diffusion and histopathologic tissue damage (39).

2. The blood oxygenation level-dependent (BOLD) method relies on similar but weaker perivascular susceptibility gradients induced by intravascular deoxyhemoglobin in the "resting" brain (40,41). Deoxyhemoglobin in intact erythrocytes is paramagnetic, whereas oxyhemoglobin is not. Local neuronal activation increases blood flow, which increases local intravascular oxyhemoglobin and elevates signal by decreasing the signal-suppressing effects of deoxyhemoglobin. No exogenous contrast agent is used, and rapid CBV changes can be measured. The BOLD method is the most widely used functional MR imaging technique for studying activation of the cerebral cortex with both GRE and SE echo-planar imaging.

3. T1-weighted imaging methods that are directly sensitive to cerebral blood flow changes have also been described but have had limited application to date (40). One method uses in-

Figure 11. Diffusion and perfusion. **(a)** Echo-planar SE T2-weighted image (5-mm-thick sections, 256 × 128 matrix [1.5 × 1.5-mm pixels], two excitations) shows a left frontal anaplastic astrocytoma with high-signal-intensity white matter edema extending posteriorly (arrow). **(b)** Diffusion map derived with a diffusion-weighted Stejskal-Tanner echo-planar SE imaging technique from multiplanar images (4,000/135, 50-msec diffusion gradient pulses, 5-mm-thick sections, 2.5-mm gap, 256 × 128 matrix [1.5 × 1.5-mm pixels], two excitations) obtained without motion artifact in an unrestrained patient in 64 seconds by using six gradient steps (0–10 mT/m; b values, 0–730 sec/mm²) (35). The gradient factor b is proportional to Larmor frequency, gradient strength, and gradient duration (36). Apparent diffusion coefficients (ADCs) (in square millimeters per second) were calculated as the slope of the semi-log plot of signal intensity versus b. The map depicts high diffusion rates as high signal intensity. The left frontal tumor shows heterogeneous diffusion rates that correspond to both high and low signal intensity on the T2-weighted image **(a)**. The highest rates in tissue are seen in the area of white matter edema (arrow). Cerebrospinal fluid and free fluid in the left frontal fluid collection show the highest diffusion rates (35). **(c)** Perfusion map of cerebral blood volume (CBV), derived from 30 sequential multisection echo-planar GRE images (2,000/60, 30° flip angle, 5-mm-thick sections, 2.5-mm gap, 256 × 128 matrix [1.5 × 1.5-mm pixels], one excitation) acquired during bolus injection of gadopentetate dimeglumine (Magnevist; Berlex Laboratories, Wayne, NJ). A time-intensity curve was traced for each pixel through the 30 images obtained at each section location, and the area under the curve was taken as the relative CBV. High CBV values are shown as high signal intensity. The CBV of the left frontal tumor is mixed and is highest centrally. This pattern does not show a simple correspondence to the signal intensity on the T2-weighted image **(a)** or to the diffusion map **(b)**. The area of white matter edema shows very low CBV (arrow).

a.

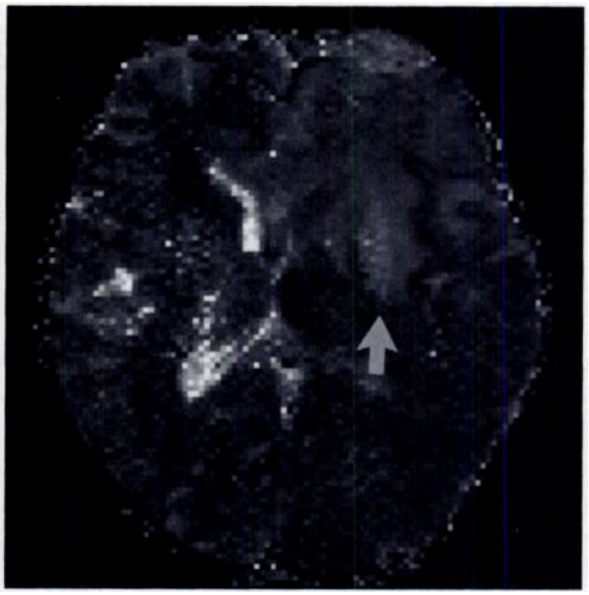

b.

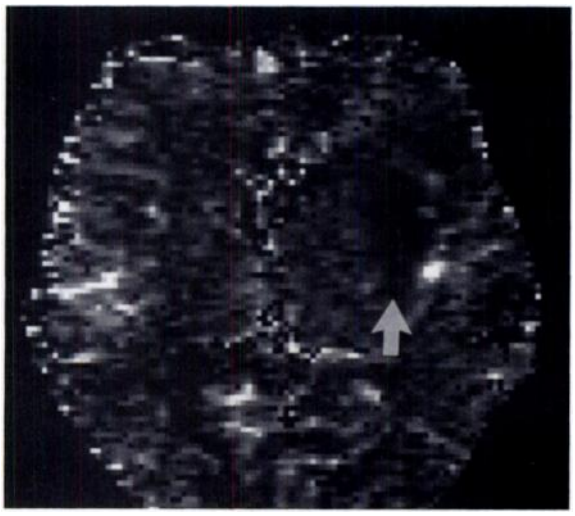

c.

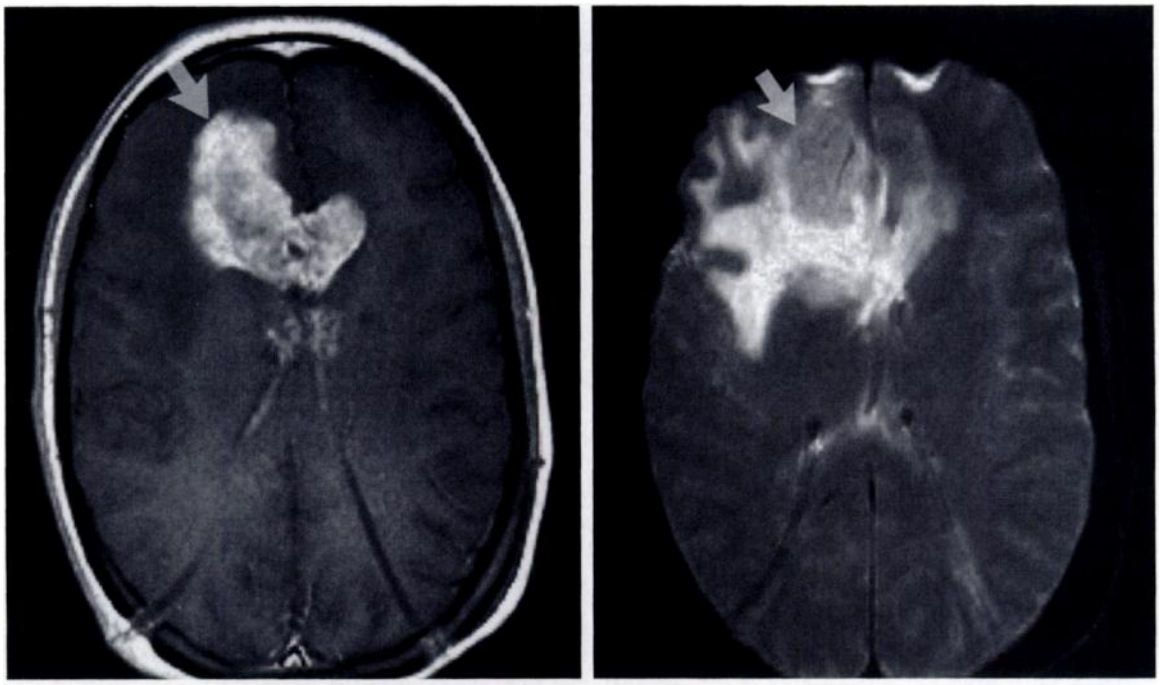

a. b.

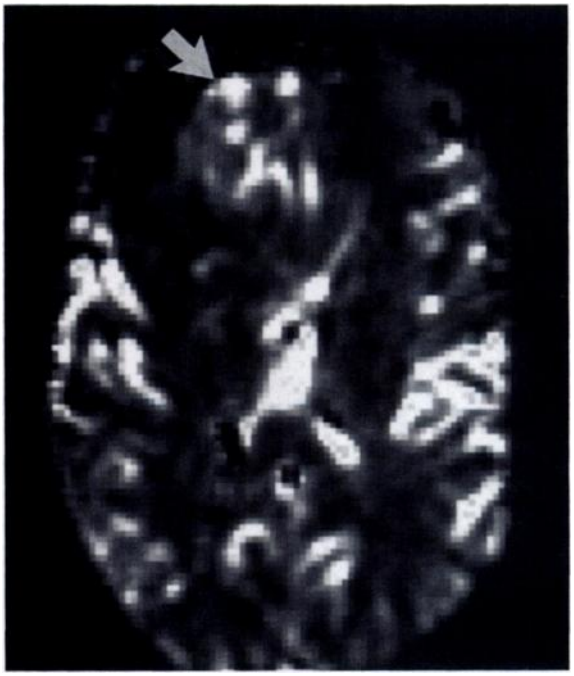

c.

Figure 12. Perfusion in a high-grade recurrent right frontal anaplastic astrocytoma with extension across the genu of the corpus callosum. **(a)** SE T1-weighted image (450/11, 7-mm-thick sections, 256 × 192 matrix [0.9 × 1.2-mm pixels], one excitation) obtained after injection of gadopentetate dimeglumine shows marked homogeneous enhancement of the tumor (arrow). **(b)** Echo-planar SE T2-weighted image (4,000/75, 7-mm-thick sections, 512 × 128 matrix [0.8 × 1.5-mm pixels], four excitations) shows intermediate signal intensity within the tumor mass (arrow) and high-signal-intensity white matter edema extending posteriorly. **(c)** Perfusion CBV map derived from 64 sequential multisection echo-planar GRE images (1,500/60, 30° flip angle, 7-mm-thick sections, eight contiguous sections, 256 × 128 matrix [1.5 × 1.5-mm pixels], one excitation) acquired during bolus injection of gadopentetate dimeglumine (0.1 mmol/kg). Elevation of CBV is seen in the region of the enhancing right frontal anaplastic astrocytoma (arrow), especially in comparison with the contralateral frontal lobe. The area of white matter edema shows relatively low CBV.

version pulse T1 "tagging" of blood protons as they flow into the echo-planar image and may allow accurate quantitation of cerebral blood flow (42).

Although conventional fast GRE techniques can be used to image cerebral perfusion, they are restricted to a small number of sections and, at low flip angles, show prominent cortical vein flow effects. Echo-planar imaging of cerebral perfusion allows multisection, whole-brain imaging and a choice of GRE, SE, or IR techniques.

In addition to perfusion imaging, fast echo-planar imaging is ideally suited for diffusion imaging because macroscopic motion is "frozen," which allows detection of the microscopic motion of diffusing water protons in tissue (36,43) (Figs 6, 11). Application of echo-planar diffusion imaging to early detection of cerebral ischemia and intracranial tumor characterization has been described. Echo-planar imaging diffusion techniques show reduced water diffusion in acute cerebral ischemia and, with echo-planar imaging perfusion studies, allow earlier detetection of ischemic lesions than do other MR imaging techniques, as early as 10-30 minutes after onset (39). Echo-planar diffusion imaging of intracranial tumors aids discrimination between cystic and solid lesions and may allow specific identification of primary central nervous system lymphoma on the basis of its low apparent diffusion coefficient values (35). Because diffusion measurements are uniquely sensitive to temperature changes, echo-planar diffusion imaging has also been suggested as a noninvasive method of monitoring tissue heating in laser surgery and hyperthermia (44,45).

■ SUMMARY

Fast echo-planar imaging is achieved by means of rapid gradient switching, which maps all phase and frequency points in k space during a single echo period. Images with resolution and contrast similar to those of conventional MR images can be obtained by using multishot acquisitions, complex k-space mapping, and standard SE, GRE, and IR pulse sequences. Specialized hardware and software are needed to meet the stringent technical requirements of single-shot echo-planar imaging. Safety issues concern the effects of rapid gradient switching on neuronal and cardiac tissue. The three major advantages of echo-planar imaging over conventional imaging are (*a*) reduced imaging time with the potential for improved patient throughput, (*b*) reduced motion artifact, and (*c*) the ability to image rapid physiologic and kinetic processes. These capabilities are opening new fields of study for MR imaging, such as evaluation of cerebral perfusion, diffusion, and functional activation, as described here, and applications in cardiac, abdominal, and real-time imaging, as discussed in detail elsewhere.

■ REFERENCES

1. Cohen MS, Fordham J. Developments in cardiac magnetic resonance imaging. Invest Radiol 1993; 28(suppl 4):S32-S37.
2. Poncelet BP, Weisskoff RM, Wedeen VJ, Brady TJ, Kantor H. Time of flight quantification of coronary flow with echo-planar MRI. Magn Reson Med 1993; 30:447-457.
3. Wendland MF, Saeed M, Masui T, Derugin N, Higgins CB. First pass of an MR susceptibility contrast agent through normal and ischemic heart: gradient-recalled echo-planar imaging. JMRI 1993; 3:755-760.
4. Goldberg MA, Hahn PF, Saini S, et al. Value of T1 and T2 relaxation times from echoplanar MR imaging in the characterization of focal hepatic lesions. AJR 1993; 160:1011-1017.
5. Schwartz LH, Koutcher JA, Panicek DM, Heelan RT, Burt M, Bains MS. Echo planar imaging of adrenal masses (abstr). AJR 1994; 162(P):23.
6. Poncelet BP, Wedeen VJ, Weisskoff RM, Cohen MS. Brain parenchyma motion: measurement with cine echo-planar MR imaging. Radiology 1992; 185:645-651.
7. Riederer SJ, Tasciyan T, Farzaneh F, Lee JN, Wright RC, Herfkens RJ. MR fluoroscopy: technical feasibility. Magn Reson Med 1988; 8:1-15.
8. Frahm J, Gyngell ML, Hanicke W. Rapid scan techniques. In: Stark DD, Bradley WG. Magnetic resonance imaging. St Louis, Mo: Mosby, 1992; 165-203.
9. Wehrli FW. Fast-scan magnetic resonance. New York, NY: Raven, 1991.
10. Wehrli FW. Introduction to fast MR imaging. In: Syllabus: a categorical course in new techniques in MR. Oak Brook, Ill: American Society of Neuroradiology, 1992; 11-21.
11. Wood ML. K-space: the final frontier. In: Syllabus: a categorical course in new techniques in MR. Oak Brook, Ill: American Society of Neuroradiology, 1992; 126-133.
12. Petersson JS, Christoffersson JO, Golman K. MRI simulation using the k-space formalism. Magn Reson Imaging 1993; 11:557-568.
13. Cohen MS, Weisskoff RM. Ultra-fast imaging. Magn Reson Imaging 1991; 9:1-37.
14. Angwin D. Resonant vs. non-resonant gradient amplifier technologies for MRI. Wilmington, Mass: Advanced NMR Systems, 1993.
15. Mansfield P. Multiplanar image formation using NMR spin echoes. J Phys Chem 1977; 10:L55.

16. Mansfield P, Pykett IL. Biological and medical imaging by NMR. J Magn Reson 1978; 29:355-373.
17. Ordidge RJ, Coxon R, Howseman A, et al. Snapshot head imaging at 0.5 T, using the echo planar technique. Magn Reson Med 1988; 8: 110-115.
18. Feinberg DA, Hale JD, Watts JC, Kaufman L, Mark A. Halving MR imaging time by conjugation: demonstration at 3.5 kG. Radiology 1986; 161:527-531.
19. Margosian PM. Faster MR imaging: imaging with half the data. Health Care Instrum 1986; 1:195-197.
20. Butts K, Riederer SJ, Ehman RL, Thompson RM, Jack CR. Interleaved echo planar imaging on a standard MRI system. Magn Reson Med 1994; 31:67-72.
21. McKinnon GC. Ultrafast interleaved gradient-echo-planar imaging on a standard scanner. Magn Reson Med 1993; 30:609-616.
22. Oshio K, Jolesz FA. Fast T1-weighted imaging with multiexcitation EPI (abstr). JMRI 1994; 4(P):37-38.
23. Harvey PR, Mansfield P. Resonant trapezoidal gradient generation for use in echo-planar imaging. Magn Reson Imaging 1994; 12:93-100.
24. McNally JM, Eastwood LM. Enhanced gradients drive image quality improvements. MR, July/August 1993; 37-40.
25. Weber DM. Non-resonant EPI gradients will enhance conventional MRI. MR, September/October 1993; 29-32.
26. Weber DM. Echo planar imaging. In: MR applications guide. Milwaukee, Wis: GE Medical Systems, 1993.
27. Budinger TF, Fischer H, Hentschel HE, et al. Neural stimulation dB/dt thresholds for frequency and number of oscillations using sinusoidal magnetic gradient fields (abstr). In: Book of abstracts: Society of Magnetic Resonance in Medicine 1990. Berkeley, Calif: Society of Magnetic Resonance in Medicine, 1990; 276.
28. Cohen MS, Weisskoff RM, Rzedzian RR, Kantor HL. Sensory stimulation by time-varying magnetic fields. Magn Reson Med 1990; 14:409-414.
29. Safety parameter action levels. In: Guidance for content and review of 510(k) applications for magnetic resonance imaging devices. Attachment I. Rockville, Md: Center for Devices and Radiological Health, U.S. Food and Drug Administration, August 2, 1988; 1-2.
30. Mansfield P, Harvey PR. Limits to neural stimulation in echo-planar imaging. Magn Reson Med 1993; 29:746-758.
31. Schmitt F, Wielopolski P, Fischer H, Edelman RR. Peripheral stimulations and their relation to gradient pulse shapes. Presented at the second meeting of the Society of Magnetic Resonance, San Francisco, Calif, August 6-12, 1994.
32. DeLaPaz RL, Krol G, O'Malley B, Davilla M. Comparison of EPI and FSE for clinical brain MR imaging (abstr). In: Proceedings of the Society of Magnetic Resonance in Medicine. Berkeley, Calif: Society of Magnetic Resonance in Medicine, 1993; 1435.
33. Yoon MS, Johnson LA, Mosher AA, et al. Sensitivity and specificity of echo-planar imaging for detection of neuropathology (abstr). JMRI 1992; 2(P):123.
34. Functional MRI of the brain, SMRM/SMRI workshop, June 17-19, 1993. Magn Reson Med 1993; 30:405-408.
35. DeLaPaz RL, Knott A, Rohan MS, Matuzek M. Diffusion-weighted echo-planar imaging of brain tumors (abstr). Radiology 1993; 189 (P):109.
36. Le Bihan D, Turner R. Diffusion and perfusion in nuclear magnetic resonance imaging. In: Potchen EJ, Haacke EM, Siebert JE, Gottschalk A, eds. Magnetic resonance angiography: concept and applications. St Louis, Mo: Mosby, 1993; 323-342.
37. Rosen BR, Belliveau JW, Vevea JM, Brady TJ. Perfusion imaging with NMR contrast agents. Magn Reson Med 1990; 14:249-266.
38. Aronen HJ, Gazit IE, Louis DN, et al. Cerebral blood volume maps of gliomas: comparison with tumor grade and histologic findings. Radiology 1994; 191:41-51.
39. Kucharczyk J, Vexler ZS, Roberts TP, et al. Echo-planar perfusion-sensitive MR imaging of acute cerebral ischemia. Radiology 1993; 188: 711-717.
40. Kwong KK, Belliveau JW, Chesler DA, et al. Dynamic magnetic resonance imaging of human brain activity during primary sensory stimulation. Proc Natl Acad Sci U S A 1992; 89: 5675-5679.
41. Ogawa S, Menon RS, Tank DW, et al. Functional brain mapping of blood oxygenation level-dependent contrast magnetic resonance imaging. Biophys J 1993; 64:803-812.
42. Edelman RR, Sievert B, Wielopolski P, Pearlman J, Warach S. Noninvasive mapping of cerebral perfusion by using EPISTAR MR angiography (abstr). JMRI 1994; 4(P):68.
43. Moseley ME, de Crespigny A, Chew WM. Diffusion/perfusion magnetic resonance imaging. Neuroimaging Clin North Am 1992; 2:693-718.
44. Jolesz FA, Bleier AR, Jakab P, Ruenzel PW, Huttl K, Jako GJ. MR imaging of laser-tissue interactions. Radiology 1988; 168:249-253.
45. Le Bihan D, Delannoy J, Levin RL. Temperature mapping with MR imaging of molecular diffusion: application to hyperthermia. Radiology 1989; 171:853-857.